



Two-way coupled
simulation of
tropospheric ozone

Y.-Y. Yan et al.

Improved simulation of tropospheric ozone by a global-multi-regional two-way coupling model system

Y.-Y. Yan¹, J.-T. Lin¹, J. Chen¹, and L. Hu²

¹Laboratory for Climate and Ocean-Atmosphere Studies, Department of Atmospheric and Oceanic Sciences, School of Physics, Peking University, Beijing 100871, China

²School of Engineering and Applied Sciences, Harvard University, Cambridge, MA 02138, USA

Received: 13 August 2015 – Accepted: 10 September 2015 – Published: 23 September 2015

Correspondence to: J.-T. Lin (linjt@pku.edu.cn)

Published by Copernicus Publications on behalf of the European Geosciences Union.

Title Page

Abstract

Introduction

Conclusions

References

Tables

Figures



Back

Close

Full Screen / Esc

Printer-friendly Version

Interactive Discussion



Abstract

Small-scale nonlinear chemical and physical processes over pollution source regions affect the global ozone (O_3) chemistry, but these processes are not captured by current global chemical transport models (CTMs) and chemistry-climate models that are limited by coarse horizontal resolutions (100–500 km, typically 200 km). These models tend to contain large (and mostly positive) tropospheric O_3 biases in the Northern Hemisphere. Here we use a recently built two-way coupling system of the GEOS-Chem CTM to simulate the global tropospheric O_3 in 2009. The system couples the global model (at 2.5° long. \times 2° lat.) and its three nested models (at 0.667° long. \times 0.5° lat.) covering Asia, North America and Europe, respectively. Benefiting from the high resolution, the nested models better capture small-scale processes than the global model alone. In the coupling system, the nested models provide results to modify the global model simulation within respective nested domains while taking the lateral boundary conditions from the global model.

Due to the “coupling” effects, the two-way system significantly improves the tropospheric O_3 simulation upon the global model alone, as found by comparisons with a suite of ground (1420 sites from WDCGG, GMD, EMEP, and AQS), aircraft (HIPPO and MOZAIC), and satellite measurements (two OMI products). Compared to the global model alone, the two-way coupled simulation enhances the correlation in day-to-day variation of afternoon mean O_3 with the ground measurements from 0.53 to 0.68, and it reduces the mean model bias from 10.8 to 6.7 ppb in annual average afternoon O_3 . Regionally, the coupled model reduces the bias by 4.6 ppb over Europe, 3.9 ppb over North America, and 3.1 ppb over other regions. The two-way coupling brings O_3 vertical profiles much closer to the HIPPO (for remote areas) and MOZAIC (for polluted regions) data, reducing the tropospheric (0–9 km) mean bias by 3–10 ppb at most MOZAIC sites and by 5.3 ppb for HIPPO profiles. The two-way coupled simulation also reduces the global tropospheric column ozone by 3.0 DU (9.5 %, annual mean), bringing them closer to the OMI data in all seasons. Simulation improvements

Two-way coupled simulation of tropospheric ozone

Y.-Y. Yan et al.

Title Page

Abstract

Introduction

Conclusions

References

Tables

Figures



Back

Close

Full Screen / Esc

Printer-friendly Version

Interactive Discussion



are more significant in the northern hemisphere, and are primarily a result of improved representation of urban-rural contrast and other small-scale processes.

The two-way coupled simulation also reduces the global tropospheric mean hydroxyl radical by 5% with enhancements by 5% in the lifetimes of methyl chloroform (from 5.58 to 5.87 yr) and methane (from 9.63 to 10.12 yr), bringing them closer to observation-based estimates. Improving model representations of small-scale processes are a critical step forward to understanding the global tropospheric chemistry.

1 Introduction

Tropospheric ozone (O_3) is a critical pollutant and the primary source of the hydroxyl radical (OH, the dominant atmospheric oxidant). Tropospheric ozone comes from stratosphere-troposphere exchange (STE) and photochemical production, and is destructed by chemical loss and dry deposition to the ground. Current global chemical transport models (CTMs) and chemistry-climate models simulate the spatiotemporal variations of ozone and its precursors, facilitating a global-scale source attribution analysis to improve mitigation strategies (Lin et al., 2014; HTAP, 2010; Monks et al., 2015). However, global models are limited by coarse horizontal resolutions (100–500 km, typically 200 km), and they cannot resolve the fine-scale processes controlling the formation, transport and removal of ozone and its precursors. This limitation may be a major contributor to the significant ozone biases found in previous studies, such as the positive biases in the Northern Hemisphere. (Lin et al., 2008; Stevenson et al., 2006; Fiore et al., 2009; Reidmiller et al., 2009; Young et al., 2013).

The coarse global models underrepresent many resolution-dependent processes. Ozone simulations greatly depend on horizontal resolutions due to its nonlinear dependence on concentrations of nitrogen oxides ($NO_x = NO + NO_2$) and non-methane volatile organic compounds (NMVOCs) (Sillman et al., 1990). Natural (biogenic and lightning) emissions are often calculated online by the models driven by resolution-specific meteorological conditions. Coarse-resolution global models cannot resolve the

Two-way coupled simulation of tropospheric ozone

Y.-Y. Yan et al.

Title Page

Abstract

Introduction

Conclusions

References

Tables

Figures



Back

Close

Full Screen / Esc

Printer-friendly Version

Interactive Discussion



The rest of the paper is organized as follows. Section 2 describes the two-way coupled model system. Section 3 presents the ground, aircraft and OMI measurements. Section 4 compares the tropospheric budgets of ozone and related species between the coupled system and the global CTM alone. The section also illustrates the resolution-dependent nonlinear chemical and physical processes to explain the simulation differences. Section 5 compares the simulated tropospheric ozone with measurements, focusing on daily, seasonal and vertical variability of ozone to demonstrate the superiority of the coupled system upon the global model alone. Section 6 concludes the present study.

2 Two-way coupled GEOS-Chem model system

The current global-multi-regional two-way coupled model system (http://wiki.seas.harvard.edu/geos-chem/index.php/Two-way_coupling_between_global_and_nested_GEOS-Chem_models) is built on version 9-02 of GEOS-Chem. In this system, both the global and three nested CTMs are driven by the GEOS-5 assimilated meteorological fields from the National Aeronautic and Space Administration (NASA) Global Modeling and Assimilation Office (GMAO). The GEOS-5 data on the native 0.667° long. \times 0.5° lat. grid are used directly to drive the nested models. To drive the global model, the meteorological data are regridded to a reduced resolution at 2.5° long. \times 2° lat. All models have 47 vertical layers, with about 10 layers of ~ 0.13 km thick below 850 hPa.

In the coupling system, all global and nested models are run with the full Ox-NOx-VOC-CO-HOx gaseous chemistry (Mao et al., 2013), the Linoz stratospheric ozone scheme (McLinden et al, 2000), and online aerosol calculations. Based on Lin et al. (2012), we have modified the chemical mechanism as follows. The reaction constants for OH + NO₂ follow Mollner et al. (2010) for low- and high-pressure limits, i.e., $k_0 = 1.48 \times 10^{-30} \times (T/300)^{-3} \text{ cm}^6 \text{ molecule}^{-2} \text{ s}^{-1}$, and $k_{\text{inf}} = 2.58 \times 10^{-11} \text{ cm}^3 \text{ molecule}^{-1} \text{ s}^{-1}$. Aerosol uptake of the hydroperoxyl radical (HO₂) ac-

Two-way coupled simulation of tropospheric ozone

Y.-Y. Yan et al.

Title Page

Abstract

Introduction

Conclusions

References

Tables

Figures



Back

Close

Full Screen / Esc

Printer-friendly Version

Interactive Discussion



**Two-way coupled
simulation of
tropospheric ozone**

Y.-Y. Yan et al.

Title Page

Abstract

Introduction

Conclusions

References

Tables

Figures



Back

Close

Full Screen / Esc

Printer-friendly Version

Interactive Discussion



counts for its self-reaction in aqueous particles (Thornton et al., 2008). Over the continental boundary layer, the uptake rate is fixed at 0.07 to account for catalysis by transition metal ions (TMIs) (Thornton et al., 2008). Over China, however, the HO₂ uptake rate is assumed to be at least 0.2 to account for the much higher fraction of TMIs in Chinese aerosols (Lin et al., 2012); the large uptake rate is supported by recent observations (Taketani et al., 2012). The uptake of nitrogen pentoxide (N₂O₅) on aerosols follows Evans and Jacob (2005) parameterization, but the uptake rate is reduced by 10 times based on more recent estimates (Bertram et al., 2009; Brown et al., 2009). Vertical mixing in the planetary boundary layer (PBL) employs a non-local scheme (Holtzlag and Boville, 1993; Lin and McElroy, 2010). Model convection adopts the Relaxed Arakawa-Schubert scheme (Rienecker et al., 2008). For the STE of ozone within the nested domains, we adjust the nested model simulations to approximate the global model results by halving the Linoz ozone production rate in the stratosphere, as we focus on the processes that affect tropospheric ozone. This adjustment does not affect the tropospheric radiation influx, which is constrained by monthly TOMS/SBUV ozone data (http://acdb-ext.gsfc.nasa.gov/Data_services/merged/).

The two-way coupling system employs the PKUCPL coupler to integrate all models. Yan et al. (2014) presents a detailed description and evaluation of the coupling mechanism. Briefly, the coupler takes global model results for all chemical concentrations to update the lateral boundary conditions (LBCs) of nested models. The coupler simultaneously replaces global model results in the troposphere within the nested domains by nested model results, after a mass-conserved area-weighted grid conversion procedure. The model information is exchanged every three hours; a higher exchange frequency at one hour leads to similar results. All model simulations proceed in parallel under the two-way coupling framework. The chemistry time step is 30 min in the global model and 20 min in the nested models; and the transport time step is half of the chemistry time step for all models. Chemical and transport processes are simulated in sequence: transport + chemistry + transport, transport + chemistry + transport, and so forth.

Two-way coupled simulation of tropospheric ozone

Y.-Y. Yan et al.

Title Page

Abstract

Introduction

Conclusions

References

Tables

Figures



Back

Close

Full Screen / Esc

Printer-friendly Version

Interactive Discussion



For our focused analysis in 2009, both the two-way coupled system and the global model alone are run from July 2008 through December 2009, allowing for a 6-month spin-up period in 2008. All models in the two-way coupling framework proceed in parallel with eight-core (Intel(R) Xeon(R) CPU X7550 at 2.00 GHz) OpenMP parallelization for each model; a total of 32 cores are used for the coupled system and eight for the global model alone. The wall-clock time of the coupled system is slightly higher (by < 2 %) than that of the slowest model, the North American nested model, due to some overhead for data exchange. On this relatively old and slow computer, it takes about 15 days for the coupled system to finish one simulation year. Initial conditions of chemicals are regridded from a simulation at 5° long. × 4° lat. conducted from 2005.

2.1 Model emissions

Table 1 summarizes the prescribed anthropogenic and biomass burning emissions. Global anthropogenic emissions are taken from the Emission Database for Global Atmospheric Research (EDGAR) v4.2 inventory for carbon monoxide (CO) and NO_x. Anthropogenic emissions of NMVOCs use as default the REanalysis of the TROpospheric chemical composition (RETRO) monthly global inventory for 2000, as implemented by Hu et al. (2015). These global inventories are further replaced by regional inventories over Asia, North America and Europe. Emission data include monthly or seasonal variability.

Monthly biomass burning emissions are taken from the Global Fire Emissions Database version 3 (GFED3) (van der Werf et al., 2010). Other natural emissions (lightning NO_x, soil NO_x, and biogenic NMVOCs) are parameterized and calculated on-the-fly based on model meteorology; these emissions are thus resolution-dependent.

Table 2 shows slight differences in global total emissions of ozone precursors (CO, NO_x, and NMVOCs) between the global model alone and the two-way coupled system. In the coupled system, global emissions from all sources are about 878 Tg yr⁻¹ for CO, 45.5 TgN yr⁻¹ for NO_x and 723 TgC yr⁻¹ for NMVOCs. These values are larger than those in the global model by about 0.9, 0.7 and 6.5 %, respectively. Greater emis-

sion differences are found for biogenic NMVOCs (by 6.9 %) and fertilizer soil NO_x (by 25.4 %), reflecting strong resolution dependence.

Figure 1 shows the spatial distributions of annual NMVOCs and NO_x emissions in the nested models (first and third columns) and the global model (second and fourth columns). The nested and global models exhibit similar spatial patterns for NMVOCs emissions. Summed over a given nested domain, the nested models have higher emissions of NMVOCs than the global model by 16–48 %, mainly a result of stronger isoprene emissions. The spatial patterns of NO_x emissions differ greatly between the nested and global models, with local emission spikes much more obvious in the nested models, although the regional totals are similar (within 5 %). These differences in model representations of NO_x and NMVOCs emissions profoundly affect the simulated ozone chemistry.

3 Ground, aircraft and OMI measurements

3.1 Ground measurements from WDCGG, GMD, EMEP and AQS

We employ four measurement networks to evaluate the modeled ground-level ozone mixing ratios in 2009. As shown in Fig. 4, these networks contain hourly ozone measurements from a total of 1420 urban, suburban or remote sites from WDCGG (64 sites, <http://ds.data.jma.go.jp/gmd/wdogg/cgi-bin/wdogg/catalogue.cgi>), GMD (12 sites, <http://www.esrl.noaa.gov/gmd/>), EMEP (130 sites, <http://www.nilu.no/projects/ccc/emepdata.html>), and AQS (1214 sites, http://aqsd1.epa.gov/aqsweb/aqstmp/airdata/download_files.html). For model evaluation, we derive the afternoon (12:00–18:00 LT, local time) mean ozone mixing ratios from the hourly data; the quantity is close to the maximum 8 h average ozone targeted by ambient air quality standards. Modeled afternoon ozone are sampled from the lowest layer (centered at ~ 0.065 km) in grid cells covering the ground sites, and are sampled from the hourly outputs coincident with available measurements.

Two-way coupled simulation of tropospheric ozone

Y.-Y. Yan et al.

Title Page

Abstract

Introduction

Conclusions

References

Tables

Figures



Back

Close

Full Screen / Esc

Printer-friendly Version

Interactive Discussion



et al. (2010a,b) with modifications as described in Kim et al. (2013), and is referred to as OMI/LIU hereafter. For OMI/LIU, errors for individual TCO retrievals are typically 2–5 DU (Liu et al., 2010). Validation against ozonesonde data show that mean OMI/LIU TCO agrees with ozonesonde data to within 2 DU for both the tropics (30° S to 30° N) and northern mid-latitudes (30°–60° N), but with season-dependent biases, varying from –0.8 DU in summer (JJA) to 2.1 DU in winter (DJF) for 30° S–30° N, and varying from –0.1 DU in JJA to 3 DU in DJF for 30–60° N (X. Liu, personal communication, 2015). The second product is the OMI/MLS dataset that subtracts the OMI total column ozone by the MLS stratospheric ozone (Ziemke et al., 2011). Ziemke et al. (2011) validated the OMI/MLS data against the Southern Hemisphere Additional OZonesondes (SHADOZ) and the World Ozone and Ultraviolet radiation Data Center (WOUDC) ozonesonde measurements. They found that, on average, the monthly mean OMI/MLS tropospheric ozone mixing ratio is smaller than the ozonesonde data by about 1 ppb (2%), with large seasonal dependence and a root mean square error at 6–8 ppb. For the present analysis, we average these two independent TCO datasets to reduce data uncertainties; this leads to a third dataset referred to as OMI_MEAN.

We use the monthly mean OMI products for 2009. The OMI/LIU dataset is on a 2.5° long. × 2° lat. grid. The OMI/MLS product provides data at 1.25° long. × 1° lat. from 60° S to 60° N. We calculate the OMI_MEAN TCO after re-gridding the OMI/MLS data to match OMI/LIU. Data polarward of 60° are discarded due to higher uncertainty. Modeled monthly mean TCO are calculated from all daily data at the OMI overpass time (13:00–15:00 LT). These OMI products and model simulations differ between each other in definitions of tropopause height and days of valid data. To examine the effect of different tropopause heights, we re-calculated in a test analysis the OMI/LIU, OMI_MEAN and model TCO by applying the OMI/MLS tropopause. The resulting bias of the global model relative to OMI_MEAN (2.8 DU, 8.9%) is similar to the bias without adjusting the tropopause (2.9 DU, 9.2%). The differences in days of valid data also have a marginal effect, as confirmed by examining the TCO difference between OMI/MLS and global model simulation sampled from days with valid OMI/MLS data

(note that the OMI/MLS product also provides daily data for such analysis). The calculated TCO difference (3.9 DU; 12.8 %) is close to the difference (4.0 DU; 13.1 %) without sampling model results.

4 Effects of two-way coupling on simulated tropospheric budgets of ozone and related species

This section examines the effect of two-way coupling on the simulated tropospheric ozone budget in 2009 (Sect. 4.1), with additional discussions on NO_x , CO, NMVOCs, OH, and lifetimes of methane and methyl chloroform (MCF) (Sect. 4.2). The two-way coupling affects the model simulation primarily through its impact on the nonlinear chemistry, followed by the resolution dependence of natural emission magnitudes and other resolution-dependent processes (Yan et al., 2014). In Sect. 4.3, we use a box model to help illustrate the GEOS-Chem simulated nonlinear ozone chemistry and its dependence on model resolution. The importance of other resolution-dependent processes is briefly discussed in Sect. 4.4.

4.1 Tropospheric ozone budget

Table 3 contrasts the global tropospheric O_3 budgets in 2009 simulated by the two-way coupled system against those by the global model alone. The chemical production and loss are calculated for the odd oxygen family ($\text{O}_x = \text{O}_3 + \text{O} + \text{NO}_2 + 2\text{NO}_3 + 3\text{N}_2\text{O}_5 + \text{PANs} + \text{HNO}_3 + \text{HNO}_4$), following Wu et al. (2007). The chemical production of O_x is mainly driven by reactions of NO with peroxy radicals, and the chemical loss is mostly due to the $\text{O}(^1\text{D}) + \text{H}_2\text{O}$ reaction and reactions of ozone with OH and HO_2 . The coupled system produces slightly higher (by $\sim 1.0\%$) chemical loss and production of O_x than the global model alone. Ozone dry deposition in the coupled system (867 Tg) is smaller by 1.7 % than the global model alone (882 Tg). The STE of ozone in the coupled simulation (478 Tg) is also lower than

Two-way coupled simulation of tropospheric ozone

Y.-Y. Yan et al.

Title Page

Abstract

Introduction

Conclusions

References

Tables

Figures



Back

Close

Full Screen / Esc

Printer-friendly Version

Interactive Discussion



the global model alone (488 Tg) by 2.0 %, partly compensating for the weaker deposition.

Table 3 shows that the coupled system produces a tropospheric ozone burden at 348 Tg, about 9.4 % lower than the burden simulated by the global model alone (384 Tg). Correspondingly, the lifetime of tropospheric ozone in the coupled system (burden divided by sink = 23.5 days) is shorter than that in the global model (26.1 days) by 9.9 %. The large reduction in ozone burden and lifetime, despite the small change in chemical production and loss of O_x , reflects a faster chemical evolution of ozone on a per molecule basis. Although both lifetimes calculated here are broadly consistent with previous studies (19.9–25.5 days from ACCMIP (Young et al., 2013) and 17.3–25.9 days from ACCENT; Stevenson et al., 2006), the reduction due to our model coupling indicates a significant effect of model resolution.

Table 4 shows the seasonal dependence of ozone burden and O_x chemical loss and production. The global model alone produces the largest chemical loss in the northern hemisphere (NH) summer (1252 Tg) and the smallest loss in winter (1036 Tg). The coupled model reduces the chemical loss by 1.2 % (to 1237 Tg) in NH summer, due to a lower ozone abundance overcompensating for a higher per-molecule loss rate. In winter, the coupled model enhances the loss by 2.3 % (to 1060 Tg), because a higher per-molecule loss rate from reactions with NO_x more than offsets a lower ozone abundance. By comparison, the coupled model slightly increases the chemical production by 0.3–1.3 % in all seasons.

4.2 NO_x , CO, NMVOCs, OH, methane lifetime, and MCF lifetime

Table 3 shows that the two-way coupling also significantly affects the tropospheric burdens of ozone-related species. Burdens of NMVOCs (10.2 TgC, see footnote of Table 3 for species included), NO_x (0.176 TgN) and CO (398 Tg) in 2009 are higher than those simulated by global model alone by 1.0, 4.1 and 10.8 %, respectively. Table 3 also shows that the global annual mean air-mass weighted tropospheric OH simulated by the two-way coupled system is lower by 5.0 % than that simulated by the global model

alone (1.12 vs. $1.18 \times 10^6 \text{ cm}^{-3}$). The sensitivity of OH to model resolution is broadly consistent with previous studies (Yan et al., 2014; Wild and Prather, 2006; Valin et al., 2011). In particular, Yan et al. (2014) showed a similar OH reduction by 4% via the two-way coupling based on an earlier version of GEOS-Chem (v8-3-02).

Table 3 further presents methane and MCF lifetimes due to reactions with the tropospheric OH. The lifetime calculation follows the formulae used by Yan et al. (2014); it accounts for the grid-box specific air mass, temperature-dependent reaction constant, OH content, and vertical gradients of methane and MCF with an adjustment coefficient of 0.97 for methane (Predoi-Cross et al., 2006) and 0.92 for MCF (Prather et al., 2012). The coupled system leads to longer lifetimes than the global model alone, by about 5.2% (from 5.58 to 5.87 yr) for MCF and 5.1% (from 9.63 to 10.12 yr) for methane. These results are closer to the observation-based estimates of MCF lifetime (6.0 ± 0.4 yr from Prinn et al., 2005; 6.3 ± 0.4 yr from Prather et al., 2012) and methane lifetime (10.2 ± 0.8 yr from Prinn et al., 2005; 11.2 ± 1.3 yr from Prather et al., 2012).

4.3 Illustrating the nonlinear ozone chemistry and resolution dependence

To illustrate the resolution dependence in simulating the nonlinear ozone chemistry, we conduct additional nested model simulations for July 2008 in a “one-way” nesting mode. Here “one-way” means that the nested models take the LBCs from the global model without affecting the global model simulation, i.e., as in a typical nested (regional) model framework. Our analysis is focused on the amount of NO_x relative to NMVOCs that affects the nonlinear ozone chemistry (e.g., Sillman et al., 1990). As detailed in Appendix A, we convert all NMVOCs to “effective” propane, according to their different capabilities in producing ozone, to facilitate inter-regional and inter-model comparisons.

Note that we only analyze the “one-way” nested model simulations in the initial month (July 2008). Also, by comparing the global and “one-way” nested models, our analysis in this section does not include the “coupling” effect, i.e., the feedback from the nested

Two-way coupled simulation of tropospheric ozone

Y.-Y. Yan et al.

Title Page

Abstract

Introduction

Conclusions

References

Tables

Figures



Back

Close

Full Screen / Esc

Printer-friendly Version

Interactive Discussion



**Two-way coupled
simulation of
tropospheric ozone**

Y.-Y. Yan et al.

Title Page

Abstract

Introduction

Conclusions

References

Tables

Figures



Back

Close

Full Screen / Esc

Printer-friendly Version

Interactive Discussion



to the global model. Our previous study on CO shows that the “one-way” nested model produces a nested-domain-average tropospheric mean CO level that is higher than the “two-way” coupled system by about 10 %, indicating a strong “coupling” effect (Yan et al., 2014). Further research is needed to fully distinguish the effect of model “coupling” (feedback) for ozone simulations over pollution source regions from the sole effect of finer resolution.

Figure 2a, e and i show the horizontal distributions of monthly mean daily average ground-level “effective” propane in July 2008 over the three nested domains (Asia, North America, and Europe) simulated by the one-way nested models. Large amounts of “effective” propane (10–100 ppbC) exist over East China, northern India, Southeast Asia, and the eastern US. The “effective” propane levels do not exceed 20 ppb over most of Europe. The global model produces a similar distribution of “effective” propane as the nested models; in particular, both global and nested models produce large NMVOC concentrations over many areas dominated by biogenic sources (Fig. 2b, f and j).

The spatial patterns of NO_x simulated by the one-way nested models (Fig. 2c, g and k) differ drastically from the patterns of “effective” propane, due to differences in their dominant sources (anthropogenic for NO_x vs. biogenic for NMVOCs). Figure 2c, g and k show that the NO_x levels range from more than 30 ppb over northern East China to below 1 ppb over most of the US and Europe. The high- NO_x spikes are obvious at polluted locations. The distribution of NO_x simulated by the global model (Fig. 2d, h and l) differs from that simulated by the nested models (Fig. 2c, g and k). In particular, the global model results in much more diluted NO_x , largely removing the contrast between polluted locations and their surroundings (e.g., urban vs. rural) seen from the nested models. The global model also produces much lower NO_x levels over East China than the nested models, despite their similar emission magnitudes (Fig. 1), reflecting the resolution-dependent nonlinear chemistry.

Figure 3 further shows the ratio of “effective” propane to NO_x , an indicator of ozone production regime, simulated by the global and nested models. The “effective” propane / NO_x ratio not only exhibits drastic variability across the three nested do-

mains, but it also differs largely between the one-way nested models (Fig. 3a, d and g) and the global model (Fig. 3b, e and h). The contrast in the ratio between polluted and cleaner surrounding areas is apparent in the nested models but hardly visible in the global model. Over East China, the “effective” propane / NO_x ratio in the nested model is much lower than the ratio in the global model (comparing Fig. 3a and b). Over Northern China Plain (115° E–125° E, 35–45° N), the ratio in the nested model ranges from 0.8 to 107 (Fig. 3a), much lower than the ratio (13.9–128) in the global model (Fig. 3b). As a consequence, the amount of ozone produced is affected by model resolution.

Figure 3c, f and i show the differences in daily mean ground-level ozone in July 2008 between the one-way nested models and the global model alone. Compared to the global model, the one-way nested models produce lower ozone concentrations over East China (by 6.1 ppb or 15.5%; averaged over 105–125° E, 20–40° N), the eastern US (by 1.0 ppb or 3.2%; 100–80° W, 30–50° N) and Europe (by 1.3 ppb or 3.7%; 15° W to 45° E, 30–70° N). The ozone reduction from the global to the nested models exceeds 10 ppb in many places of East China, Los Angeles, and parts of the coast of the Gulf of Mexico due to stronger titration by NO_x. The ozone reduction is despite the higher (natural) emissions in the nested models (Fig. 1); and it indicates that in this case, the spatial distribution of ozone precursor emissions is more important to the ozone chemistry than the magnitude of emissions. Appendix B further discusses the ozone chemistry for three exemplary cities within the nested domains; it clearly shows that high-resolution nested models better capture the urban-rural contrast in ozone production regime.

Therefore, when results from the nested models are allowed to modify the global model simulation via the “two-way” coupling mechanism, the simulation improvements for ozone and other species (due to increased model resolution over pollutant source regions) can be transported to outside the nested domain to exhibit a global impact. This aspect has been demonstrated for CO (Yan et al., 2014).

Two-way coupled simulation of tropospheric ozone

Y.-Y. Yan et al.

Title Page

Abstract

Introduction

Conclusions

References

Tables

Figures



Back

Close

Full Screen / Esc

Printer-friendly Version

Interactive Discussion



4.4 Importance of resolution-dependent factors other than chemistry

Figure 3c, f and i show that the one-way nested models produce larger amounts of ground-level ozone than the global model over West China and the western US (Fig. 3c, f and i). The enhancements are most evident over uneven terrains of the Tibetan Plateau and along the Rocky Mountains, due to an enhancement in vertical transport from the global to the nested models (Chen et al., 2009; Zhang et al., 2011). For the tropospheric mean ozone, the nested model simulations are close to the global model results over West China (within 0.04 ppb over West China (80–100° E, 30–50° N; and within 0.2 ppb over the western US (120–110° W, 30–50° N)). The nested models also better represent the complex terrains along the coasts, partly contributing to its lower ozone than the global model.

5 Evaluation of modeled tropospheric ozone against ground, aircraft and satellite measurements

5.1 Surface ozone

As shown in Fig. 4, most ground measurement sites are located in the US (1214 sites from AQS) and Europe (130 sites from EMEP). Averaged over the US AQS sites, the measured annual mean afternoon (12:00–18:00 LT) mean ozone is 35.8 ppb in 2009. The afternoon ozone is slightly higher over Europe, about 37.7 ppb averaged over the EMEP sites. The ozone level is highest over Asia, with a value of 43.1 ppb averaged over the seven WDCGG sites. The afternoon ozone from the 17 WDCGG sites worldwide is about 33.8 ppb on average.

Figure 5 shows the horizontal distributions of annual mean afternoon ozone biases simulated by the global model alone (Fig. 5a, c and e) and by the two-way coupled system (Fig. 5b, d and f), relative to the four ground networks. The global model tends to overestimate the ozone concentrations (biases range from –5 to 25 ppb), with a

Two-way coupled simulation of tropospheric ozone

Y.-Y. Yan et al.

[Title Page](#)[Abstract](#)[Introduction](#)[Conclusions](#)[References](#)[Tables](#)[Figures](#)[Back](#)[Close](#)[Full Screen / Esc](#)[Printer-friendly Version](#)[Interactive Discussion](#)

mean bias at +10.8 ppb globally, +10.5 ppb over the US, and +12.1 ppb over Europe. The positive biases exceed 15 ppb at several high-elevation sites of the western US (Fig. 5c) and some coastal sites of Europe (Fig. 5e). These results are broadly consistent with previous multi-model evaluation for the HTAP (Reidmiller et al., 2009) and ACENT (Dentener et al., 2006) projects that showed an ensemble mean positive bias at 10–20 ppb over the summertime eastern US and 15–20 ppb over South Asia, respectively. Similar model biases are also found from our previous evaluation of MOZART and GEOS-Chem over the US (Lin et al., 2008; Lin and McElroy, 2010). Compared to the global model alone, the two-way coupled system generally reduces the ozone bias worldwide (Fig. 5b, d, and f). The positive bias is reduced to 6.7 ppb globally, 6.6 ppb over the US, and 7.5 ppb over Europe. The bias reduction is apparent at several WD-CGG sites over the North Pacific and North Atlantic (comparing Fig. 5a and b) and over the eastern US (comparing Fig. 5c and d).

Figure 6 compares the modeled and measured day-to-day time series of regional mean afternoon ozone in 2009 for six regions in the US (from AQS) and two regions in Europe (from EMEP). The regions are defined in Fig. 5c–f, as separated by blue lines. In general, the measured ozone levels are highest in spring and summer (Fig. 6, black lines), due to stronger STE and/or higher chemical production. Both the global model and the two-way coupled system capture the seasonal variation of measured ozone (Fig. 6, blue and red lines). The global model alone tends to overestimate the observations; the annual mean bias is 9–15 ppb for any given region. Seasonally, the overestimate is largest in winter over the western US (Fig. 6a and b), in summer over the eastern US and northern Europe (Fig. 6c–g), and in fall over southern Europe (Fig. 6h). The two-way coupled simulation reduces the ozone biases in most days and regions (Fig. 6, red lines). On a seasonal mean basis, the largest reductions occur in winter (2–8 ppb for individual regions), due mainly to much enhanced titration by NO_x (not shown). The bias reductions are smallest in summer (< 3 ppb). This is partly because ozone production from the increased natural precursor emissions (Table 2) compensate to some extent for a stronger chemical ozone loss. Furthermore, although the

**Two-way coupled
simulation of
tropospheric ozone**

Y.-Y. Yan et al.

Title Page

Abstract

Introduction

Conclusions

References

Tables

Figures



Back

Close

Full Screen / Esc

Printer-friendly Version

Interactive Discussion



et al., 2013). The coupled system produces lower ozone concentrations in the troposphere (0–9 km) than the global model alone. This translates to ozone bias reductions by 3–11 ppb at most MOZAIC sites (in the polluted areas) and by 5.3 ppb for HIPPO profiles (in the remote areas), averaged over 0–9 km. These improvements are a result of interactions between improved ozone simulations over pollution source regions and improved simulations of background ozone, as initially driven by a higher resolution over the source regions.

Figure 9 further shows the ozone profiles in individual seasons of 2009 at Frankfurt. With several hundred profiles in each season, this site allows for a detailed seasonal analysis. Again, although both the two-way coupled system and the global model alone capture the general vertical distribution of ozone in any given season, the coupled system leads to much lower biases below 9 km.

5.3 Tropospheric column ozone

Figure 10 presents the horizontal distributions of TCO in individual seasons from OMI/MLS, OMI/LIU, their average OMI_MEAN, the two-way coupled system, and the global model alone. OMI/MLS and OMI/LIU produce similar seasonal and spatial distributions of TCO, with lower values in the tropics but higher values in the northern mid-latitudes (especially in the Northern Hemisphere (NH) summer and fall) and near 30° S. In general, OMI/LIU produces higher TCO values than OMI/MLS by 0.8 DU (2.8%), 1.6 DU (5.3%), 3.8 DU (11.9%) and 2.8 DU (9.0%) in NH spring, summer, fall and winter, respectively. These differences are broadly consistent with the uncertainties in OMI/MLS and OMI/LIU discussed in Sect. 3.3. We thus use their average, OMI_MEAN, for model evaluation.

Figure 10 shows that both the global model alone and the coupled system reproduce the general seasonal and spatial structures of OMI_MEAN TCO. The global model tends to overestimate the seasonal TCO in OMI_MEAN, with a global mean bias of 4.4 DU (15.2%), 3.4 DU (10.9%), 2.2 DU (6.5%), and 1.6 DU (4.9%) in NH spring, summer, fall, and winter, respectively. The positive bias is more significant in the NH

Two-way coupled simulation of tropospheric ozone

Y.-Y. Yan et al.

Title Page

Abstract

Introduction

Conclusions

References

Tables

Figures



Back

Close

Full Screen / Esc

Printer-friendly Version

Interactive Discussion



(annual mean bias = 3.6 DU) than in the Southern Hemisphere (SH, bias = 2.2 DU). The large NH overestimate was found also for the ACCMIP model ensemble (Young et al., 2013). Compared to the global model alone, the coupled system reduces the annual average TCO by 3.0 DU (9.5 %) globally, by 3.8 DU in the NH, and by 2.1 DU in the SH. The coupled system also leads to TCO values closer to OMI_MEAN, with a global mean bias of 1.2 DU (4.1 %) in NH spring, 0.1 DU (0.3 %) in summer, -0.7 DU (-2.1 %) in fall and -0.7 DU (-2.2 %) in winter. The model improvements are more significant in the NH.

6 Conclusions

This study evaluate the tropospheric ozone in 2009 simulated by a two-way coupled system integrating the global GEOS-Chem CTM (at 2.5° long. × 2° lat.) and its three fine-resolution nested models (at 0.667° long. × 0.5° lat.) covering Asia, North America and Europe. The nested models better capture nonlinear small-scale chemical, physical and other processes within the nested domains; and the two-way coupling allows such improvements to have a global impact. The coupled system requires an amount of computational resource affordable for most users, i.e., 32 cores compared to eight cores for the global model alone for a similar wall-clock time.

The coupled system is compared against the coarse global model alone, by employing a suite of ozone measurements in 2009 from four ground networks (WDCGG, GMD, AQS in the US, and EMEP in Europe, with 1420 sites), MOZAIC and HIPPO aircraft campaigns, and two OMI TCO products. Model evaluation clearly indicates the superiority of the two-way coupled system. Compared to the global model alone, the coupled system produces afternoon (12:00–18:00 LT) mean ground-level ozone much closer to the measurements. On an annual mean basis, the model bias is reduced by 4.1 ppb (from 10.8 to 6.7 ppb) globally, by 3.9 ppb (from 10.5 to 6.6 ppb) over the US, and by 4.6 ppb (from 12.1 to 7.5 ppb) over Europe. The coupled system also enhances the correlation to the measurements in day-to-day ozone variability from 0.53 to 0.68,

**Two-way coupled
simulation of
tropospheric ozone**

Y.-Y. Yan et al.

Title Page

Abstract

Introduction

Conclusions

References

Tables

Figures

◀

▶

◀

▶

Back

Close

Full Screen / Esc

Printer-friendly Version

Interactive Discussion



lar NMVOC to propane. The simulation period is set at a typical clear-sky summer-time midday (12:00–13:00 LT; air pressure = 1013 hPa; daytime mean air temperature = 295 K; $[H_2O] = 1.0 \times 10^4$ ppm; daytime mean solar radiation = 278 W m^{-2}). The initial conditions are 30 ppb for ozone, 150 ppb for CO, and 10 ppbC for the NMVOC to be tested. The initial condition of NO_x varies from 0.2 to 30 ppb across different simulations. Each simulation is done for a given NMVOC, with other MNVOCs turned off.

Figure A1 shows the large dependence of $P_{O_3}(\text{NMVOC})/P_{O_3}(\text{C}_3\text{H}_8)$ on initial concentrations of NO_x , for each of the nine primarily emitted NMVOCs considered in GEOS-Chem. These NMVOCs are converted to produce the “effective” propane. Depending on the initial condition of NO_x (from 0.2 to 30 ppb), the $P_{O_3}(\text{NMVOC})/P_{O_3}(\text{C}_3\text{H}_8)$ ratio spans 1–3 orders of magnitude for any given NMVOC. The ratios for propene (PRPE, representing all alkenes) and formaldehyde (CH_2O) vary from 1–2 for $NO_x = 0.2$ ppb to about 50 for $NO_x = 10$ –20 ppb. The ratio for isoprene (ISOP) is close to 0.1 for $NO_x = 0.2$ ppb, increasing to unity for $NO_x = 1.2$ ppb and to a high value of 40 for $NO_x = 30$ ppb. The low ratio for isoprene in low- NO_x conditions is associated with the depletion of OH.

Appendix B: Nonlinear ozone chemistry at three representative cities

As shown in Table A1, we choose three representative cities to illustrate the effect of model resolution in simulating the nonlinear ozone chemistry: Beijing, China (with a large change in NO_x concentrations from the global to the one-way nested model, averaged over the city and its surroundings), Minneapolis, the US (with a strong contrast in NO_x between urban and rural areas), and Arcachon, France (with a greater difficulty in the global model in identifying the coastline). The NO_x and NMVOC concentrations in July 2008 from the one-way nested models are compared against those from the global model alone.

Commission for the support to the MOZAIC project (1994–2003) and the preparatory phase of IAGOS (2005–2012) partner institutions of the IAGOS Research Infrastructure (FZJ, DLR, MPI, KIT in Germany, CNRS, CNES, Météo-France in France and University of Manchester in United Kingdom), ETHER (CNES-CNRS/INSU) for hosting the database, the participating airlines (Lufthansa, Air France, Austrian, China Airlines, Iberia, Cathay Pacific) for the transport free of charge of the instrumentation.

References

- Auvray, M. and Bey, I.: Long-range transport to Europe: seasonal variations and implications for the European ozone budget, *J. Geophys. Res.-Atmos.*, 110, D11303, doi:10.1029/2004jd005503, 2005.
- Bertram, T. H., Thornton, J. A., Riedel, T. P., Middlebrook, A. M., Bahreini, R., Bates, T. S., Quinn, P. K., and Coffman, D. J.: Direct observations of N_2O_5 reactivity on ambient aerosol particles, *Geophys. Res. Lett.*, 36, L19803, doi:10.1029/2009gl040248, 2009.
- Bond, T. C., Bhardwaj, E., Dong, R., Jogani, R., Jung, S., Roden, C., Streets, D. G., and Trautmann, N. M.: Historical emissions of black and organic carbon aerosol from energy-related combustion, 1850-2000, *Global Biogeochem. Cy.*, 21, GB2018, doi:10.1029/2006GB002840, 2007.
- Bouwman, A. F., Lee, D. S., Asman, W. A. H., Dentener, F. J., Van Der Hoek, K. W., and Olivier, J. G. J.: A global high-resolution emission inventory for ammonia, *Global Biogeochem. Cy.*, 11, 561–587, 1997.
- Brown, S. S., Dube, W. P., Fuchs, H., Ryerson, T. B., Wollny, A. G., Brock, C. A., Bahreini, R., Middlebrook, A. M., Neuman, J. A., Atlas, E., Roberts, J. M., Osthoff, H. D., Trainer, M., Fehsenfeld, F. C., and Ravishankara, A. R.: Reactive uptake coefficients for N_2O_5 determined from aircraft measurements during the Second Texas Air Quality Study: Comparison to current model parameterizations, *J. Geophys. Res.-Atmos.*, 114, D00F10, doi:10.1029/2008jd011679, 2009.
- Chen, D., Wang, Y., McElroy, M. B., He, K., Yantosca, R. M., and Le Sager, P.: Regional CO pollution and export in China simulated by the high-resolution nested-grid GEOS-Chem model, *Atmos. Chem. Phys.*, 9, 3825–3839, doi:10.5194/acp-9-3825-2009, 2009.

Two-way coupled simulation of tropospheric ozone

Y.-Y. Yan et al.

Title Page

Abstract

Introduction

Conclusions

References

Tables

Figures



Back

Close

Full Screen / Esc

Printer-friendly Version

Interactive Discussion



**Two-way coupled
simulation of
tropospheric ozone**

Y.-Y. Yan et al.

Title Page

Abstract

Introduction

Conclusions

References

Tables

Figures



Back

Close

Full Screen / Esc

Printer-friendly Version

Interactive Discussion



Dentener, F., Stevenson, D., Ellingsen, K., van Noije, T., Schultz, M., Amann, M., Atherton, C., Bell, N., Bergmann, D., Bey, I., Bouwman, L., Butler, T., Cofala, J., Collins, B., Drevet, J., Doherty, R., Eickhout, B., Eskes, H., Fiore, A., Gauss, M., Hauglustaine, D., Horowitz, L., Isaksen, I. S. A., Josse, B., Lawrence, M., Krol, M., Lamarque, J. F., Montanaro, V., Muller, J. F., Peuch, V. H., Pitari, G., Pyle, J., Rast, S., Rodriguez, J., Sanderson, M., Savage, N. H., Shindell, D., Strahan, S., Szopa, S., Sudo, K., Van Dingenen, R., Wild, O., and Zeng, G.: The global atmospheric environment for the next generation, *Environ. Sci. Technol.*, 40, 3586–3594, doi:10.1021/es0523845, 2006.

El Amraoui, L., Attié, J.-L., Semane, N., Claeys, M., Peuch, V.-H., Warner, J., Ricaud, P., Cammas, J.-P., Piacentini, A., Josse, B., Cariolle, D., Massart, S., and Bencherif, H.: Midlatitude stratosphere – troposphere exchange as diagnosed by MLS O₃ and MOPITT CO assimilated fields, *Atmos. Chem. Phys.*, 10, 2175–2194, doi:10.5194/acp-10-2175-2010, 2010.

Emmerson, K. M. and Evans, M. J.: Comparison of tropospheric gas-phase chemistry schemes for use within global models, *Atmos. Chem. Phys.*, 9, 1831–1845, doi:10.5194/acp-9-1831-2009, 2009.

Evans, M. J. and Jacob, D. J.: Impact of new laboratory studies of N₂O₅ hydrolysis on global model budgets of tropospheric nitrogen oxides, ozone, and OH, *Geophys. Res. Lett.*, 32, L09813, doi:10.1029/2005gl022469, 2005.

Fiore, A. M., Dentener, F. J., Wild, O., Cuvelier, C., Schultz, M. G., Hess, P., Textor, C., Schulz, M., Doherty, R. M., Horowitz, L. W., MacKenzie, I. A., Sanderson, M. G., Shindell, D. T., Stevenson, D. S., Szopa, S., Van Dingenen, R., Zeng, G., Atherton, C., Bergmann, D., Bey, I., Carmichael, G., Collins, W. J., Duncan, B. N., Faluvegi, G., Folberth, G., Gauss, M., Gong, S., Hauglustaine, D., Holloway, T., Isaksen, I. S. A., Jacob, D. J., Jonson, J. E., Kaminski, J. W., Keating, T. J., Lupu, A., Marmer, E., Montanaro, V., Park, R. J., Pitari, G., Pringle, K. J., Pyle, J. A., Schroeder, S., Vivanco, M. G., Wind, P., Wojcik, G., Wu, S., and Zuber, A.: Multimodel estimates of intercontinental source-receptor relationships for ozone pollution, *J. Geophys. Res.*, 114, D04301, doi:10.1029/2008jd010816, 2009.

Hu, L., Millet, D. B., Baasandorj, M., Griffis, T. J., Travis, K. R., Tessum, C. W., Marshall, J. D., Reinhart, W. F., Mikoviny, T., Mueller, M., Wisthaler, A., Graus, M., Warneke, C., and de Gouw, J.: Emissions of C₆C₈ aromatic compounds in the United States: Constraints from tall tower and aircraft measurements, *J. Geophys. Res.-Atmos.*, 120, 826–842, doi:10.1002/2014jd022627, 2015.

**Two-way coupled
simulation of
tropospheric ozone**

Y.-Y. Yan et al.

Title Page

Abstract

Introduction

Conclusions

References

Tables

Figures



Back

Close

Full Screen / Esc

Printer-friendly Version

Interactive Discussion



Huang, X., Song, Y., Li, M., Li, J., Huo, Q., Cai, X., Zhu, T., Hu, M., and Zhang, H.: A high-resolution ammonia emission inventory in China, *Global Biogeochem. Cy.*, 26, Gb1030, doi:10.1029/2011gb004161, 2012.

Holtstlag, A. A. M., and Boville, B. A.: Local Versus Non-local Boundary-Layer Diffusion in a Global Climate Model, *J. Climate*, 6, 1825–1842, doi:10.1175/1520-0442(1993)006<1825:lvnbl>2.0.co;2, 1993.

HTAP: Hemispheric Transport of Air Pollution 2010 Executive Summary ECE/EB.AIR/2010/10 Corrected, United Nations, 2010.

Janssens-Maenhout, G., Petrescu, A. M. R., Muntean, M., and Blujdea, V.: Verifying Greenhouse Gas Emissions: Methods to Support International Climate Agreements, *The National Academies Press*, 132–133, doi:10.1080/20430779.2011.579358, 124 pp., 2010.

Kim, P. S., Jacob, D. J., Liu, X., Warner, J. X., Yang, K., Chance, K., Thouret, V., and Nedelec, P.: Global ozone-CO correlations from OMI and AIRS: constraints on tropospheric ozone sources, *Atmos. Chem. Phys.*, 13, 9321–9335, doi:10.5194/acp-13-9321-2013, 2013.

Kort, E. A., Wofsy, S. C., Daube, B. C., Diao, M., Elkins, J. W., Gao, R. S., Hints, E. J., Hurst, D. F., Jimenez, R., Moore, F. L., Spackman, J. R., and Zondlo, M. A.: Atmospheric observations of Arctic Ocean methane emissions up to 82 degrees north, *Nat. Geosci.*, 5, 318–321, doi:10.1038/ngeo1452, 2012.

Kuhns, H., Etyemezian, V., Green, M., Hendrickson, K., Mc-Gown, M., Barton, K., and Pitchford, M.: Vehicle-based road dust emission measurement – Part II: Effect of precipitation, winter-time road sanding, and street sweepers on inferred PM₁₀ emission potentials from paved and unpaved roads, *Atmos. Environ.*, 37, 4573–4582, doi:10.1016/s1352-2310(03)00529-6, 2003.

Lin, J.-T. and McElroy, M. B.: Impacts of boundary layer mixing on pollutant vertical profiles in the lower troposphere: Implications to satellite remote sensing, *Atmos. Environ.*, 44, 1726–1739, doi:10.1016/j.atmosenv.2010.02.009, 2010.

Lin, J.-T., Youn, D., Liang, X. Z., and Wuebbles, D. J.: Global model simulation of summertime US ozone diurnal cycle and its sensitivity to PBL mixing, spatial resolution, and emissions, *Atmos. Environ.*, 42, 8470–8483, doi:10.1016/j.atmosenv.2008.08.012, 2008.

Lin, J.-T., Liu, Z., Zhang, Q., Liu, H., Mao, J., and Zhuang, G.: Modeling uncertainties for tropospheric nitrogen dioxide columns affecting satellite-based inverse modeling of nitrogen oxides emissions, *Atmos. Chem. Phys.*, 12, 12255–12275, doi:10.5194/acp-12-12255-2012, 2012.

**Two-way coupled
simulation of
tropospheric ozone**

Y.-Y. Yan et al.

Title Page

Abstract

Introduction

Conclusions

References

Tables

Figures



Back

Close

Full Screen / Esc

Printer-friendly Version

Interactive Discussion



Lin, J.-T., Pan, D., Davis, S. J., Zhang, Q., He, K., Wang, C., Streets, D. G., Wuebbles, D. J., and Guan, D.: China's international trade and air pollution in the United States, *P. Natl. Acad. Sci. USA*, 111, 1736–1741, doi:10.1073/pnas.1312860111, 2014.

Liu, X., Chance, K., and Kurosu, T. P.: Improved ozone profile retrievals from GOME data with degradation correction in reflectance, *Atmos. Chem. Phys.*, 7, 1575–1583, doi:10.5194/acp-7-1575-2007, 2007.

Liu, X., Bhartia, P. K., Chance, K., Spurr, R. J. D., and Kurosu, T. P.: Ozone profile retrievals from the Ozone Monitoring Instrument, *Atmos. Chem. Phys.*, 10, 2521–2537, doi:10.5194/acp-10-2521-2010, 2010.

Mao, J., Paulot, F., Jacob, D. J., Cohen, R. C., Crounse, J. D., Wennberg, P. O., Keller, C. A., Hudman, R. C., Barkley, M. P., and Horowitz, L. W.: Ozone and organic nitrates over the eastern United States: Sensitivity to isoprene chemistry, *J. Geophys. Res.-Atmos.*, 118, 11256–11268, doi:10.1002/jgrd.50817, 2013.

Marengo, A., Thouret, V., Nedelec, P., Smit, H., Helten, M., Kley, D., Karcher, F., Simon, P., Law, K., Pyle, J., Poschmann, G., Von Wrede, R., Hume, C., and Cook, T.: Measurement of ozone and water vapor by Airbus in-service aircraft: The MOZAIC airborne program, An overview, *J. Geophys. Res.-Atmos.*, 103, 25631–25642, doi:10.1029/98jd00977, 1998.

McLinden, C. A., Olsen, S. C., Hannegan, B., Wild, O., Prather, M. J., and Sundet, J.: Stratospheric ozone in 3-D models: A simple chemistry and the cross-tropopause flux, *J. Geophys. Res.-Atmos.*, 105, 14653–14665, doi:10.1029/2000jd900124, 2000.

Mollner, A. K., Valluvadasan, S., Feng, L., Sprague, M. K., Okumura, M., Milligan, D. B., Bloss, W. J., Sander, S. P., Martien, P. T., Harley, R. A., McCoy, A. B., and Carter, W. P. L.: Rate of Gas Phase Association of Hydroxyl Radical and Nitrogen Dioxide, *Science*, 330, 646–649, doi:10.1126/science.1193030, 2010.

Monks, P. S., Archibald, A. T., Colette, A., Cooper, O., Coyle, M., Derwent, R., Fowler, D., Granier, C., Law, K. S., Mills, G. E., Stevenson, D. S., Tarasova, O., Thouret, V., von Schneidemesser, E., Sommariva, R., Wild, O., and Williams, M. L.: Tropospheric ozone and its precursors from the urban to the global scale from air quality to short-lived climate forcer, *Atmos. Chem. Phys.*, 15, 8889–8973, doi:10.5194/acp-15-8889-2015, 2015.

Prather, M. J., Holmes, C. D., and Hsu, J.: Reactive greenhouse gas scenarios: systematic exploration of uncertainties and the role of atmospheric chemistry, *Geophys. Res. Lett.*, 39, L09803, doi:10.1029/2012GL051440, 2012.

Two-way coupled simulation of tropospheric ozone

Y.-Y. Yan et al.

Title Page

Abstract

Introduction

Conclusions

References

Tables

Figures



Back

Close

Full Screen / Esc

Printer-friendly Version

Interactive Discussion



- Predoi-Cross, A., Brawley-Tremblay, M., Brown, L. R., Devi, V. M., and Benner, D. C.: Multispectrum analysis of (CH₄)-C₁₂ from 4100 to 4635 cm⁻¹: II. Air-broadening coefficients (widths and shifts), *J. Mol. Spectrosc.*, 236, 201–215, doi:10.1016/j.jms.2006.01.013, 2006.
- Prinn, R. G., Huang, J., Weiss, R. F., Cunnold, D. M., Fraser, P. J., Simmonds, P. G., McCulloch, A., Harth, C., Reimann, S., Salameh, P., O'Doherty, S., Wang, R. H. J., Porter, L. W., Miller, B. R., and Krummel, P. B.: Evidence for variability of atmospheric hydroxyl radicals over the past quarter century, *Geophys. Res. Lett.*, 32, L07809, doi:10.1029/2004gl022228, 2005.
- Proffitt, M. H. and McLaughlin, R. J.: Fast-response Dual-beam UV Absorption Ozone Photometer Suitable for Use on Stratospheric Balloons, *Rev. Sci. Instrum.*, 54, 1719–1728, doi:10.1063/1.1137316, 1983.
- Reidmiller, D. R., Fiore, A. M., Jaffe, D. A., Bergmann, D., Cuvelier, C., Dentener, F. J., Duncan, B. N., Folberth, G., Gauss, M., Gong, S., Hess, P., Jonson, J. E., Keating, T., Lupu, A., Marmer, E., Park, R., Schultz, M. G., Shindell, D. T., Szopa, S., Vivanco, M. G., Wild, O., and Zuber, A.: The influence of foreign vs. North American emissions on surface ozone in the US, *Atmos. Chem. Phys.*, 9, 5027–5042, doi:10.5194/acp-9-5027-2009, 2009.
- Rienecker, E., Ryan, J., Blum, M., Dietz, C., Coletti, L., Marin III, R., and Bissett, W. P.: Mapping phytoplankton in situ using a laser-scattering sensor, *Limnol. Oceanogr.-Meth.*, 6, 153–161, doi:10.4319/lom.2008.6.153, 2008.
- Sillman, S., Logan, J. A., and Wofsy, S. C.: The Sensitivity of Ozone to Nitrogen Oxides and Hydrocarbon in Regional Ozone Episodes, *J. Geophys. Res.-Atmos.*, 95, 1837–1851, doi:10.1029/JD095iD02p01837, 1990.
- Simone, N. W., Stettler, M. E. J., and Barrett, S. R. H.: Rapid estimation of global civil aviation emissions with uncertainty quantification, *Transport. Res. D-Tr. E.*, 25, 33–41, doi:10.1016/j.trd.2013.07.001, 2013.
- Stevenson, D. S., Dentener, F. J., Schultz, M. G., Ellingsen, K., van Noije, T. P. C., Wild, O., Zeng, G., Amann, M., Atherton, C. S., Bell, N., Bergmann, D. J., Bey, I., Butler, T., Cofala, J., Collins, W. J., Derwent, R. G., Doherty, R. M., Drevet, J., Eskes, H. J., Fiore, A. M., Gauss, M., Hauglustaine, D. A., Horowitz, L. W., Isaksen, I. S. A., Krol, M. C., Lamarque, J. F., Lawrence, M. G., Montanaro, V., Müller, J. F., Pitari, G., Prather, M. J., Pyle, J. A., Rast, S., Rodriguez, J. M., Sanderson, M. G., Savage, N. H., Shindell, D. T., Strahan, S. E., Sudo, K., and Szopa, S.: Multimodel ensemble simulations of present-day and near-future tropospheric ozone, *J. Geophys. Res.*, 111, D08301, doi:10.1029/2005jd006338, 2006.

**Two-way coupled
simulation of
tropospheric ozone**

Y.-Y. Yan et al.

Title Page

Abstract

Introduction

Conclusions

References

Tables

Figures



Back

Close

Full Screen / Esc

Printer-friendly Version

Interactive Discussion



Stevenson, D. S., Young, P. J., Naik, V., Lamarque, J.-F., Shindell, D. T., Voulgarakis, A., Skeie, R. B., Dalsoren, S. B., Myhre, G., Berntsen, T. K., Folberth, G. A., Rumbold, S. T., Collins, W. J., MacKenzie, I. A., Doherty, R. M., Zeng, G., van Noije, T. P. C., Strunk, A., Bergmann, D., Cameron-Smith, P., Plummer, D. A., Strode, S. A., Horowitz, L., Lee, Y. H., Szopa, S.,

5 Sudo, K., Nagashima, T., Josse, B., Cionni, I., Righi, M., Eyring, V., Conley, A., Bowman, K. W., Wild, O., and Archibald, A.: Tropospheric ozone changes, radiative forcing and attribution to emissions in the Atmospheric Chemistry and Climate Model Intercomparison Project (ACCMIP), *Atmos. Chem. Phys.*, 13, 3063–3085, doi:10.5194/acp-13-3063-2013, 2013.

Streets, D., Bond, T., Carmichael, G., Fernandes, S., Fu, Q., He, D., Klimont, Z., Nelson, S.,

10 Tsai, N., and Wang, M. Q.: An inventory of gaseous and primary aerosol emissions in Asia in the year 2000, *J. Geophys. Res.*, 108, 8809, doi:10.1029/2002JD003093, 2003.

Taketani, F., Kanaya, Y., Pochanart, P., Liu, Y., Li, J., Okuzawa, K., Kawamura, K., Wang, Z., and Akimoto, H.: Measurement of overall uptake coefficients for HO₂ radicals by aerosol particles sampled from ambient air at Mts. Tai and Mang (China), *Atmos. Chem. Phys.*, 12,

15 11907–11916, doi:10.5194/acp-12-11907-2012, 2012.

Thornton, J. A., Jaegle, L., and McNeill, V. F.: Assessing known pathways for HO₂ loss in aqueous atmospheric aerosols: Regional and global impacts on tropospheric oxidants, *J. Geophys. Res.-Atmos.*, 113, D05303, doi:10.1029/2007jd009236, 2008.

Thouret, V., Marengo, A., Logan, J. A., Nedelec, P., and Grouhel, C.: Comparisons of ozone measurements from the MOZAIC airborne program and the ozone sounding network at eight

20 locations, *J. Geophys. Res.-Atmos.*, 103, 25695–25720, doi:10.1029/98jd02243, 1998.

Valin, L. C., Russell, A. R., Hudman, R. C., and Cohen, R. C.: Effects of model resolution on the interpretation of satellite NO₂ observations, *Atmos. Chem. Phys.*, 11, 11647–11655, doi:10.5194/acp-11-11647-2011, 2011.

Valin, L. C., Russell, A. R., and Cohen, R. C.: Chemical feedback effects on the spatial patterns of the NO_x weekend effect: a sensitivity analysis, *Atmos. Chem. Phys.*, 14, 1–9, doi:10.5194/acp-14-1-2014, 2014.

van der Werf, G. R., Randerson, J. T., Giglio, L., Collatz, G. J., Mu, M., Kasibhatla, P. S., Morton, D. C., DeFries, R. S., Jin, Y., and van Leeuwen, T. T.: Global fire emissions and the contribution of deforestation, savanna, forest, agricultural, and peat fires (1997–2009), *Atmos. Chem. Phys.*, 10, 11707–11735, doi:10.5194/acp-10-11707-2010, 2010.

30

**Two-way coupled
simulation of
tropospheric ozone**

Y.-Y. Yan et al.

Title Page

Abstract

Introduction

Conclusions

References

Tables

Figures



Back

Close

Full Screen / Esc

Printer-friendly Version

Interactive Discussion



Vinken, G. C. M., Boersma, K. F., van Donkelaar, A., and Zhang, L.: Constraints on ship NO_x emissions in Europe using GEOS-Chem and OMI satellite NO₂ observations, *Atmos. Chem. Phys.*, 14, 1353–1369, doi:10.5194/acp-14-1353-2014, 2014.

Wild, O. and Prather, M. J.: Global tropospheric ozone modeling: Quantifying errors due to grid resolution, *J. Geophys. Res.*, 111, D11305, doi:10.1029/2005jd006605, 2006.

Wofsy, S. C.: HIAPER Pole-to-Pole Observations (HIPPO): fine-grained, global-scale measurements of climatically important atmospheric gases and aerosols, *Philos. T. Roy. Soc. A*, 369, 2073–2086, doi:10.1098/rsta.2010.0313, 2011.

Xiao, Y., J. A. Logan, D. J. Jacob, R. C. Hudman, R. Yantosca, and D. R. Blake: The global budget of ethane and regional constraints on U.S. sources, *J. Geophys. Res.*, 113, D21306, doi:10.1029/2007JD009415, 2008.

Yan, Y.-Y., Lin, J.-T., Kuang, Y., Yang, D., and Zhang, L.: Tropospheric carbon monoxide over the Pacific during HIPPO: two-way coupled simulation of GEOS-Chem and its multiple nested models, *Atmos. Chem. Phys.*, 14, 12649–12663, doi:10.5194/acp-14-12649-2014, 2014.

Young, P. J., Archibald, A. T., Bowman, K. W., Lamarque, J.-F., Naik, V., Stevenson, D. S., Tilmes, S., Voulgarakis, A., Wild, O., Bergmann, D., Cameron-Smith, P., Cionni, I., Collins, W. J., Dalsøren, S. B., Doherty, R. M., Eyring, V., Faluvegi, G., Horowitz, L. W., Josse, B., Lee, Y. H., MacKenzie, I. A., Nagashima, T., Plummer, D. A., Righi, M., Rumbold, S. T., Skeie, R. B., Shindell, D. T., Strode, S. A., Sudo, K., Szopa, S., and Zeng, G.: Pre-industrial to end 21st century projections of tropospheric ozone from the Atmospheric Chemistry and Climate Model Intercomparison Project (ACCMIP), *Atmos. Chem. Phys.*, 13, 2063–2090, doi:10.5194/acp-13-2063-2013, 2013.

Zbinden, R. M., Thouret, V., Ricaud, P., Carminati, F., Cammas, J.-P., and Nédélec, P.: Climatology of pure tropospheric profiles and column contents of ozone and carbon monoxide using MOZAIC in the mid-northern latitudes (24° N to 50° N) from 1994 to 2009, *Atmos. Chem. Phys.*, 13, 12363–12388, doi:10.5194/acp-13-12363-2013, 2013.

Zhang, L., Jacob, D. J., Downey, N. V., Wood, D. A., Blewitt, D., Carouge, C. C., van Donkelaar, A., Jones, D. B. A., Murray, L. T., and Wang, Y.: Improved estimate of the policy-relevant background ozone in the United States using the GEOS-Chem global model with 1/2° × 2/3° horizontal resolution over North America, *Atmos. Environ.*, 45, 6769–6776, doi:10.1016/j.atmosenv.2011.07.054, 2011.

Zhang, L., Jacob, D. J., Yue, X., Downey, N. V., Wood, D. A., and Blewitt, D.: Sources contributing to background surface ozone in the US Intermountain West, *Atmos. Chem. Phys.*, 14, 5295–5309, doi:10.5194/acp-14-5295-2014, 2014.

5 Zhang, Q., Streets, D. G., Carmichael, G. R., He, K. B., Huo, H., Kannari, A., Klimont, Z., Park, I. S., Reddy, S., Fu, J. S., Chen, D., Duan, L., Lei, Y., Wang, L. T., and Yao, Z. L.: Asian emissions in 2006 for the NASA INTEX-B mission, *Atmos. Chem. Phys.*, 9, 5131–5153, doi:10.5194/acp-9-5131-2009, 2009.

10 Ziemke, J. R., Chandra, S., Labow, G. J., Bhartia, P. K., Froidevaux, L., and Witte, J. C.: A global climatology of tropospheric and stratospheric ozone derived from Aura OMI and MLS measurements, *Atmos. Chem. Phys.*, 11, 9237–9251, doi:10.5194/acp-11-9237-2011, 2011.

ACPD

15, 25789–25836, 2015

Two-way coupled simulation of tropospheric ozone

Y.-Y. Yan et al.

Title Page

Abstract

Introduction

Conclusions

References

Tables

Figures



Back

Close

Full Screen / Esc

Printer-friendly Version

Interactive Discussion



Two-way coupled simulation of tropospheric ozone

Y.-Y. Yan et al.

Title Page

Abstract

Introduction

Conclusions

References

Tables

Figures



Back

Close

Full Screen / Esc

Printer-friendly Version

Interactive Discussion

**Table 1.** Anthropogenic and biomass burning emission inventories used by GEOS-Chem.

Region	Dataset	Resolution ¹	Year	Species	References and notes
Anthropogenic (fossil + biofuel) emissions					
Global	EDGAR v4.2	0.1° × 0.1°, seasonal	2008	CO, NO _x , SO ₂	Janssens-Maenhout et al. (2010)
Global	RETRO	0.5° × 0.5°, monthly	2000	NMVOCs ²	http://accent.aero.jussieu.fr/RETRO_metadata.php
Global	GEIA	1° × 1°, seasonal	1990	NH ₃	Bouwman et al. (1997)
Global	T. Bond	1° × 1°, monthly	2000	BC, OC	Bond et al. (2007)
Global	AEIC (aircraft)	1° × 1°, annual	2005	CO, NO _x , NMVOCs ² , SO ₂ , BC, OC	Simone et al. (2013)
Asia	INTEX-B	0.5° × 0.5°, monthly	2006	CO, NO _x , NMVOCs ² , SO ₂ , BC, OC	Zhang et al. (2009)
Asia	D. Streets	1° × 1°, monthly	2000	NH ₃	Streets et al. (2003)
China	MEIC	0.25° × 0.25°, monthly	2008 ³	CO, NO _x , NMVOCs ² , NH ₃ , SO ₂	Lin et al. (2015); Huang et al. (2012); http://www.meicmodel.org/
US	NEI05	4 km × 4 km, monthly and weekend/weekday	2005 ³	CO, NO _x , NMVOCs, NH ₃ , SO ₂	ftp://aftp.fsl.noaa.gov/divisions/taq/emissions_data_2005
Canada	CAC	1° × 1°, annual	2005 ³	CO, NO _x , NH ₃ , SO ₂	http://www.ec.gc.ca/pdb/cac/cac_home_e.cfm
Mexico	BRAVO	1° × 1°, annual	1999	CO, NO _x , SO ₂	Kuhns et al. (2003)
Europe	EMEP	0.5° × 0.5°, monthly	2005	CO, NO _x , NMVOCs ² , NH ₃ , SO ₂	Auvray and Bey (2005)
Biomass burning emissions					
Global	GFED3	0.5° × 0.5°, monthly	2009	CO, NMVOCs, NO _x , NH ₃ , SO ₂ , BC, OC	van der Werf et al. (2010)

¹ Before re-gridded to model horizontal resolutions. For more information, see http://wiki.seas.harvard.edu/geos-chem/index.php/Anthropogenic_emissions.

² RETRO includes PRPE, C₃H₈, ALK₄, ALD₂, CH₂O, and MEK; in the CTM, MEK emissions are further allocated to MEK (25%) and ACET (75%). AEIC, INTEX-B and MEIC include PRPE, C₂H₆, C₂H₈, ALK₄, ALD₂, CH₂O, MEK, and ACET. NEI05 includes PRPE, C₃H₈, ALK₄, CH₂O, MEK, and ACET. EMEP includes PRPE, ALK₄, ALD₂, and MEK. Emissions of C₂H₆ outside Asia are from Xiao et al. (2008). See the captions of Fig. A1 for NMVOC names.

³ Over China, emissions of NO_x are further scaled to 2009 based on the tropospheric NO₂ columns from OMI measurements (Lin, et al., 2015). Over the US and Canada, emissions of CO, NO_x and SO₂ are scaled to 2009 (http://wiki.seas.harvard.edu/geos-chem/index.php/Scale_factors_for_anthropogenic_emissions).

Two-way coupled simulation of tropospheric ozone

Y.-Y. Yan et al.

[Title Page](#)

[Abstract](#)

[Introduction](#)

[Conclusions](#)

[References](#)

[Tables](#)

[Figures](#)

[◀](#)

[▶](#)

[◀](#)

[▶](#)

[Back](#)

[Close](#)

[Full Screen / Esc](#)

[Printer-friendly Version](#)

[Interactive Discussion](#)



Table 2. Global emissions of CO, NO_x and NMVOCs in GEOS-Chem for 2009.

Total emissions ¹	Global model	Two-way model	Percentage difference
CO emissions (Tg)	869.9	877.8	0.9 %
Fossil + Biofuel	500.5	504.3	0.8 %
Biomass burning	327.6	327.3	−0.1 %
NO _x emissions (TgN)	45.2	45.5	0.7 %
Fos			
Natural Soil	5.81	5.86	0.9 %
Fertilizer Soil	0.71	0.89	25.4 %
Biomass burning	4.55	4.54	−0.2 %
Aircraft	0.51	0.51	0
NMVOCs emissions (TgC) ²	678.4	722.7	6.5 %
Fossil + Biofuel	27.8	28.1	1.1 %
Biogenic NMVOCs	640	684	6.9 %
Biomass burning	10.6	10.6	0

¹ Slight differences may exist between the two model frameworks in the prescribed anthropogenic (fossil + biofuel) and biomass burning emissions, as a result of the combination of and regridding from various inventories. The consequent impacts on model simulations are negligible.

² Emitted NMVOCs include ISOP, PRPE, C₃H₈, ALK₄, C₂H₆, ALD₂, CH₂O, ACET, and MEK. See the captions of Fig. A1 for NMVOC names.

Two-way coupled simulation of tropospheric ozone

Y.-Y. Yan et al.

Title Page

Abstract

Introduction

Conclusions

References

Tables

Figures

◀

▶

◀

▶

Back

Close

Full Screen / Esc

Printer-friendly Version

Interactive Discussion

**Table 3.** Global tropospheric budgets of ozone and related species for 2009.

	Global model	Two-way model	Percentage difference
Tropospheric budget of ozone ¹			
Chemical loss of O _x (Tg)	4491	4537	1.0%
Chemical production of O _x (Tg)	4885	4928	0.9%
Dry deposition of O _x (Tg)	909	894	-1.7%
STE of O _x (Tg) ²	515	503	-2.3%
Dry deposition of O ₃ (Tg)	882	867	-1.7%
STE of O ₃ (Tg) ²	488	478	-2.0%
O ₃ burden (Tg)	384	348	-9.4%
Mean TCO (DU)	34.5	31.5	-8.7%
O ₃ lifetime (days)	26.1	23.5	-9.9%
Tropospheric burdens and lifetimes of other species			
NO _x burden (TgN)	0.169	0.176	4.1%
NMVOCs burden (TgC) ³	10.1	10.2	1.0%
CO burden (Tg)	359	398	10.8%
OH number concentration (10 ⁶ cm ⁻³)	1.18	1.12	-5.0%
OH-related MCF lifetime (yr) ⁴	5.58	5.87	5.2%
OH-related methane lifetime (yr) ⁴	9.63	10.12	5.1%

¹ Chemical production and loss rates are calculated for the odd oxygen family (O_x = O₃ + O + NO₂ + 2NO₃ + 3N₂O₅ + PANs + HNO₃ + HNO₄, Wu et al., 2007), to exclude recycling reactions between O₃ and other O_x species. We note that O₃ accounts for over 95 % of the mass of O_x. The tropopause is defined in GEOS-5 as at the pressure where the function [0.037 - log₁₀P] reaches its first minimum above the surface (http://acmg.seas.harvard.edu/geos/wiki_docs/geos5/GEOS-5.2.0-File_Specification.pdf).

² Stratosphere-troposphere exchange is inferred from mass balance: O_x STE = O_x chemical loss + O_x dry deposition - O_x chemical production, and O₃ STE = O₃ chemical loss + O₃ dry deposition - O₃ chemical production.

³ NMVOCs for burden calculation include the emitted species only: ISOP, PRPE, C₃H₈, ALK₄, C₂H₆, ALD₂, CH₂O, ACET, and MEK. See the captions of Fig. A1 for NMVOC names.

⁴ Observation-based estimates are 10.2 ± 0.8 (Prinn et al., 2005) or 11.2 ± 1.3 (Prather et al., 2012) years for OH-related methane lifetime, and 6.0 ± 0.4 (Prinn et al., 2005) or 6.3 ± 0.4 (Prather et al., 2012) years for OH-related MCF lifetime.

Two-way coupled simulation of tropospheric ozone

Y.-Y. Yan et al.

Table 4. Global tropospheric ozone burden and O_x chemical production and loss in individual seasons of 2009.

	MAM			JJA			SON			DJF		
	GB	TW	Diff. (%)									
Chemical loss of O _x (Tg)	1087	1099	1.1 %	1252	1237	−1.2 %	1116	1141	2.2 %	1036	1060	2.3 %
Chemical production of O _x (Tg)	1197	1213	1.3 %	1446	1460	1.0 %	1199	1211	1.0 %	1042	1045	0.3 %
O ₃ burden (Tg)	374	340	−9.1 %	394	362	−8.0 %	370	339	−8.4 %	399	352	−11.7 %
Lifetime against chemical loss (O ₃ burden/O _x loss)	31.4	28.3	−9.8 %	28.7	26.7	−6.9 %	30.3	27.1	−10.5 %	35.1	30.3	−13.6 %

[Title Page](#)
[Abstract](#)
[Introduction](#)
[Conclusions](#)
[References](#)
[Tables](#)
[Figures](#)

[Back](#)
[Close](#)
[Full Screen / Esc](#)
[Printer-friendly Version](#)
[Interactive Discussion](#)


Two-way coupled simulation of tropospheric ozone

Y.-Y. Yan et al.

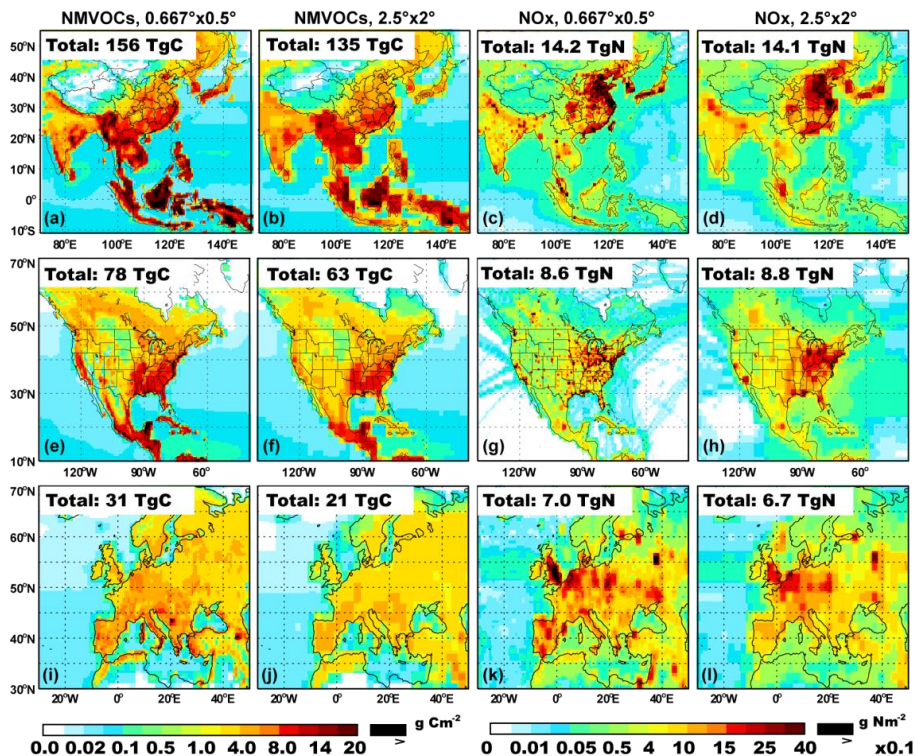


Figure 1. Total (anthropogenic + natural) emissions of NMVOCs and NO_x over Asia, North America and Europe in 2009, as represented in the nested models ($0.667^\circ \times 0.5^\circ$) and the global model ($2.5^\circ \times 2^\circ$). Values outside the upper bound of color intervals are shown in black. Color intervals are nonlinear to better present the data range; an interval without labeling represents the mean of adjacent two intervals. Also depicted in each panel is the regional total.

Title Page

Abstract Introduction

Conclusions References

Tables Figures

◀ ▶

◀ ▶

Back Close

Full Screen / Esc

Printer-friendly Version

Interactive Discussion



Two-way coupled simulation of tropospheric ozone

Y.-Y. Yan et al.

Title Page

Abstract

Introduction

Conclusions

References

Tables

Figures

◀

▶

◀

▶

Back

Close

Full Screen / Esc

Printer-friendly Version

Interactive Discussion

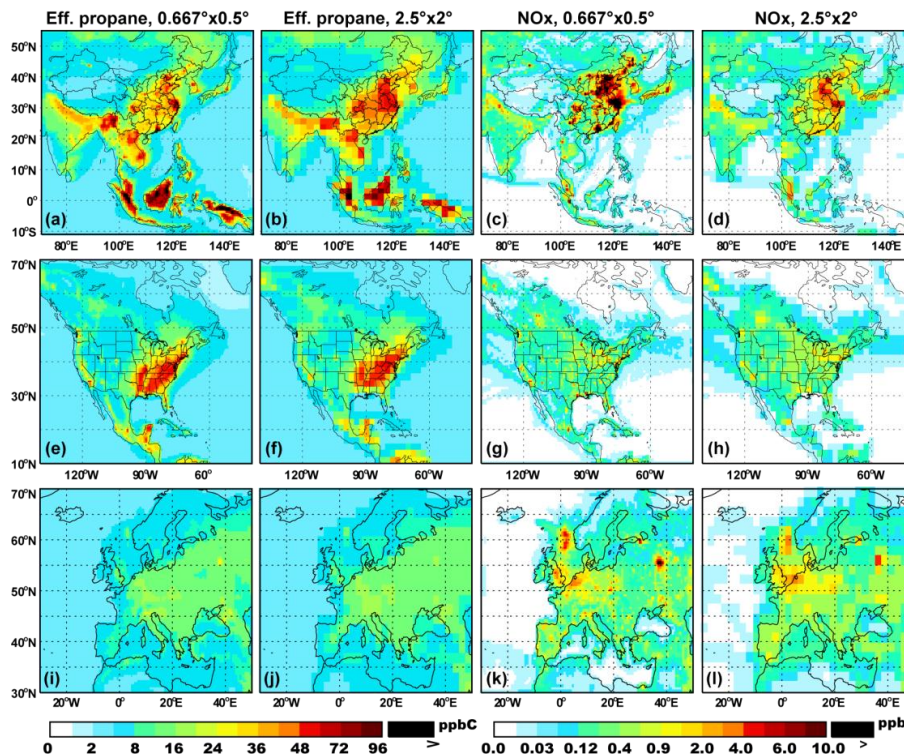


Figure 2. Daily mean mixing ratios of ground-level NO_x and “effective” propane over Asia, North America and Europe in July 2008, as simulated by the one-way nested models ($0.667^\circ \times 0.5^\circ$) and the global model ($2.5^\circ \times 2^\circ$). Values outside the upper bound of color intervals are shown in black. Color intervals are nonlinear to better present the data range; an interval without labeling represents the mean of adjacent two intervals.

Two-way coupled simulation of tropospheric ozone

Y.-Y. Yan et al.

Title Page

Abstract

Introduction

Conclusions

References

Tables

Figures



Back

Close

Full Screen / Esc

Printer-friendly Version

Interactive Discussion

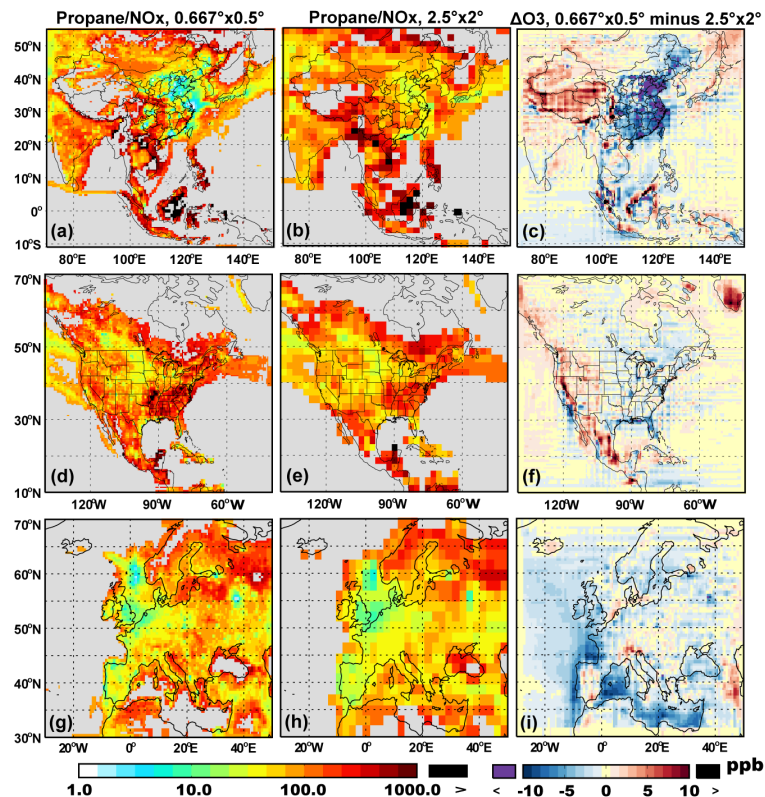


Figure 3. Ratio of daily mean “effective” propane to NO_x in July 2008 simulated by the one-way nested models ($0.667^\circ \times 0.5^\circ$, left column) and the global model ($2.5^\circ \times 2^\circ$, middle column), and the differences in daily mean ground-level ozone between the one-way nested models and the global model (right column, regridded to the nested resolution). Values outside the upper (lower) bound of color intervals are shown in black (purple). In the first two columns, color intervals are logarithmic to better present the data range, and values are masked over areas with extremely low NO_x (< 0.025 ppb) and thus weak ozone production.

Two-way coupled simulation of tropospheric ozone

Y.-Y. Yan et al.

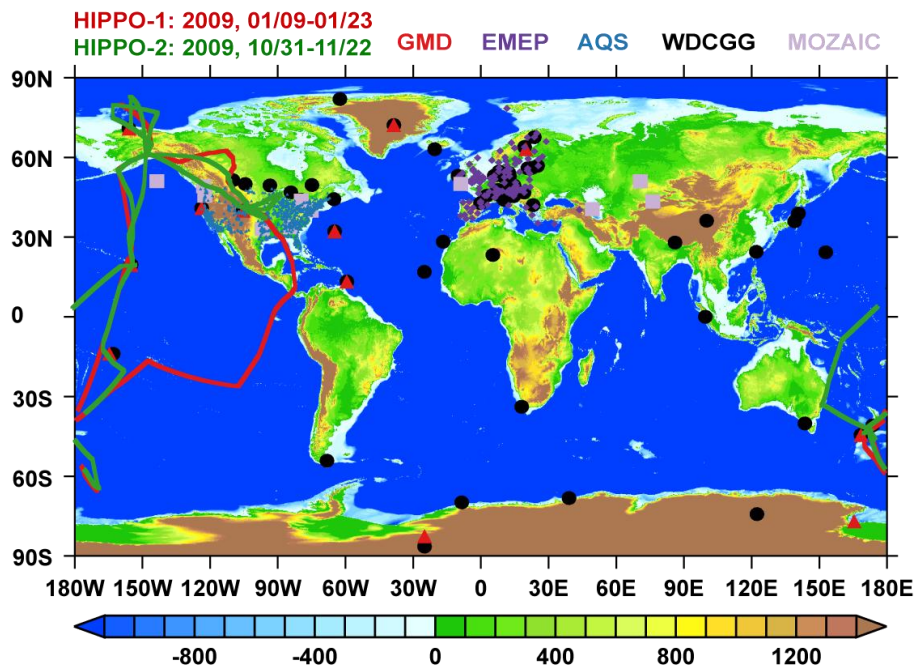


Figure 4. Sites of ground-level ozone measurements from WDCGG (black circle), GMD (red triangle), AQS (blue triangle) and EMEP (purple diamond); airports in the MOZAIK program for the tropospheric ozone profiles (pink square); and aircraft flight tracks in the HIPPO campaigns (red line for HIPPO-1, and green line for HIPPO-2). The overlaid map is the surface elevation (m) from a 2 min Gridded Global Relief Data (ETOPO2v2) available at NGDC Marine Trackline Geophysical database (<http://www.ngdc.noaa.gov/mgg/global/etopo2.html>).

Title Page

Abstract

Introduction

Conclusions

References

Tables

Figures



Back

Close

Full Screen / Esc

Printer-friendly Version

Interactive Discussion



Two-way coupled simulation of tropospheric ozone

Y.-Y. Yan et al.

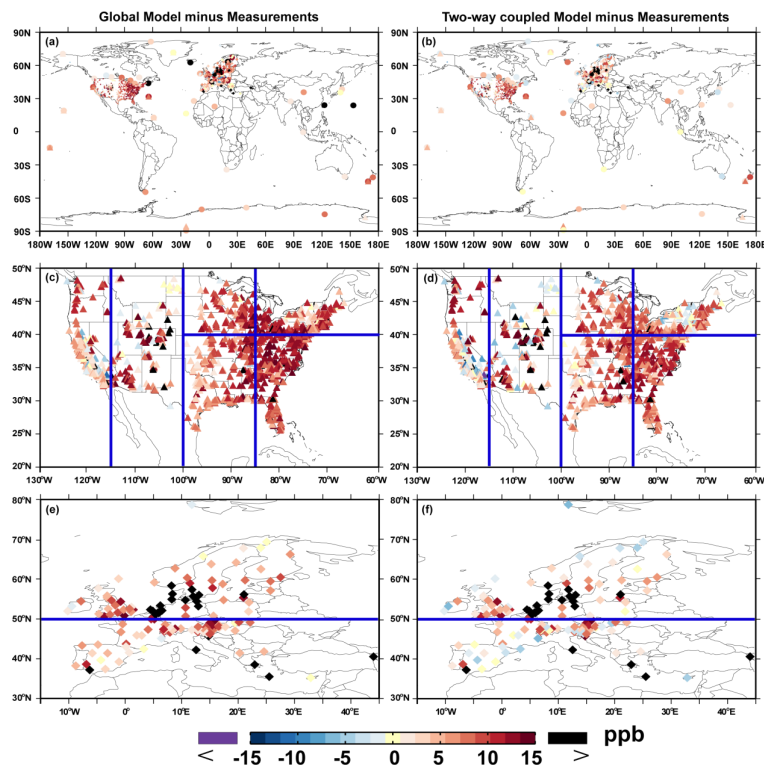


Figure 5. Anneal mean model biases in afternoon (12:00–18:00 LT) mean ground-level ozone for the global model alone (a) and the two-way coupled model (b), with respect to measurements from WDCGG, GMD, AQS and EMEP. The symbol shapes differentiate measurement networks, consistent with Fig. 4 (circle for WDCGG, large triangle for GMD, small triangle for AQS, and diamond for EMEP). The US and European domains are enlarged in (c–f) to better show spatial distributions. Blue lines separate the regions presented in Fig. 5.

Two-way coupled
simulation of
tropospheric ozone

Y.-Y. Yan et al.

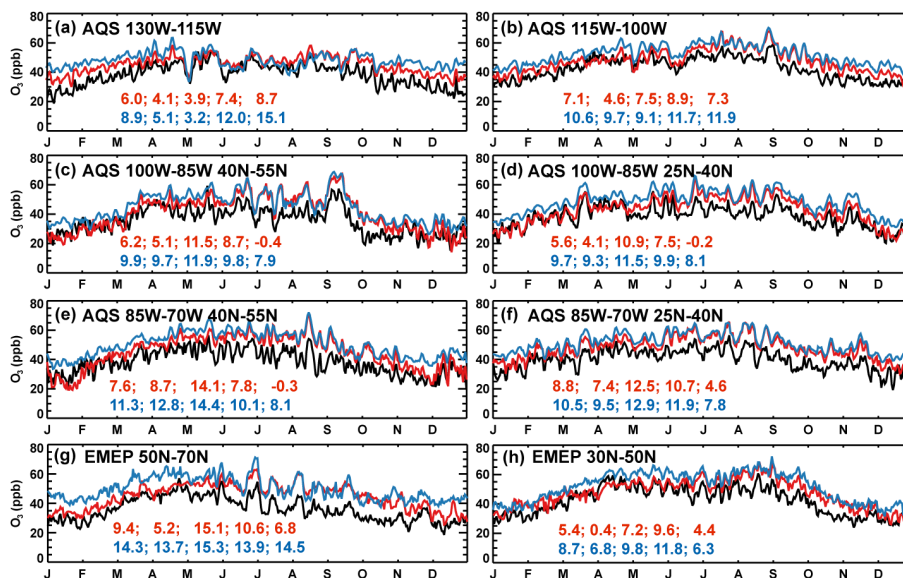


Figure 6. Time series of afternoon (12:00–18:00 LT) mean ground-level ozone from AQS and EMEP measurements (black lines) and from model simulations (red lines for two-way simulation and blue lines for global model alone). Data are averaged over individual triangular regions indicated in Fig. 5. Numbers shown in each panel are mean model biases for annual mean, spring (MAM), summer (JJA), fall (SON), and winter (DJF).

Title Page

Abstract

Introduction

Conclusions

References

Tables

Figures



Back

Close

Full Screen / Esc

Printer-friendly Version

Interactive Discussion



Two-way coupled simulation of tropospheric ozone

Y.-Y. Yan et al.

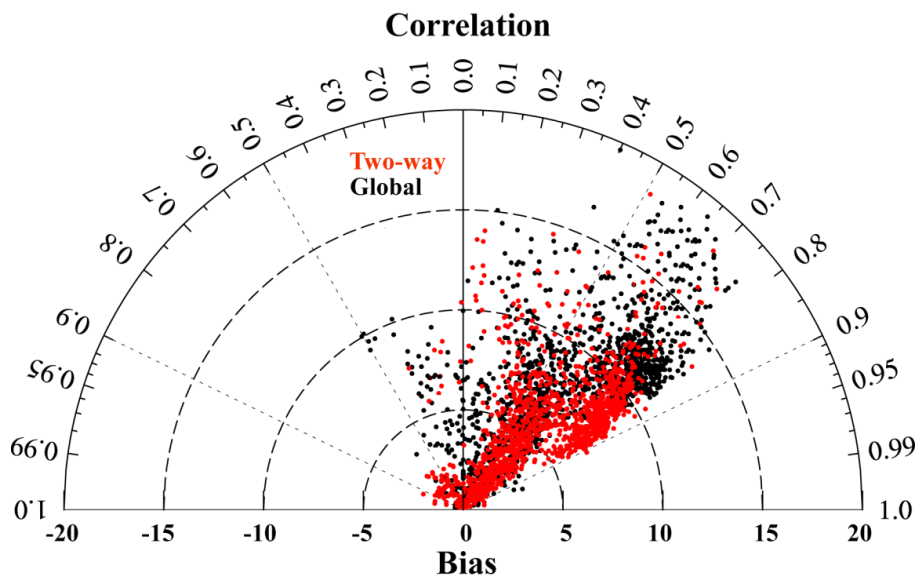


Figure 7. Mean bias and day-to-day correlation of afternoon (12:00–18:00 LT) mean ground-level ozone for model simulations with respect to measurements from WDCGG, GMD, EMEP and AQS (a total of 1420 sites and 365 site-days).

[Title Page](#)[Abstract](#)[Introduction](#)[Conclusions](#)[References](#)[Tables](#)[Figures](#)[◀](#)[▶](#)[◀](#)[▶](#)[Back](#)[Close](#)[Full Screen / Esc](#)[Printer-friendly Version](#)[Interactive Discussion](#)

Two-way coupled simulation of tropospheric ozone

Y.-Y. Yan et al.

Title Page

Abstract

Introduction

Conclusions

References

Tables

Figures



Back

Close

Full Screen / Esc

Printer-friendly Version

Interactive Discussion

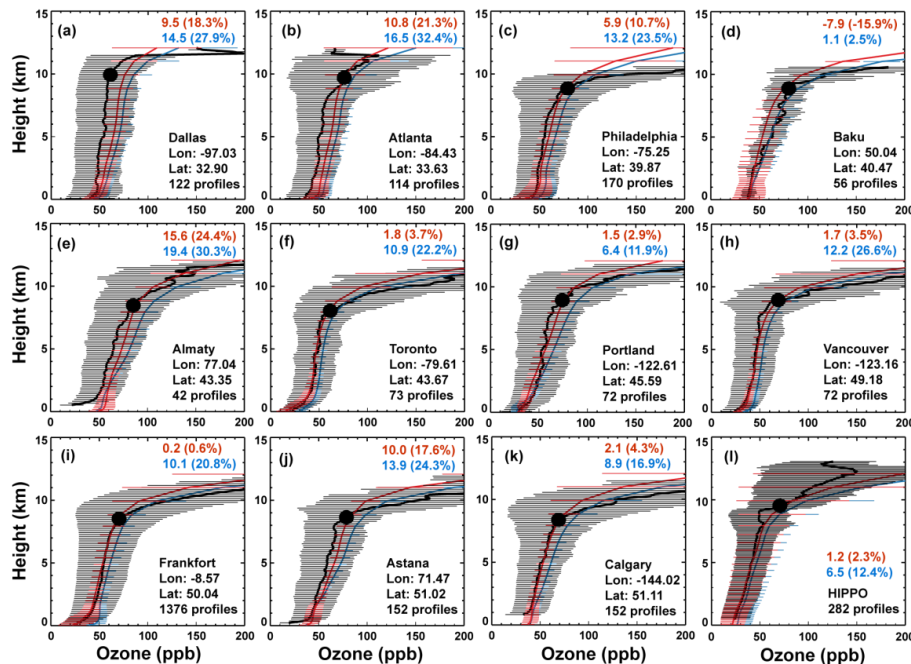


Figure 8. Measured (black) and simulated (red for two-way coupled model and blue for global model alone) vertical profiles of ozone in 2009 for the MOZAIC (a–k) and HIPPO campaigns (l). MOZAIC measurements are from the ground level (0.075 km) to the UTLS at 0.15 km intervals, as averaged over all profiles. HIPPO data are averaged over all profiles at 0.1 km intervals. Model results are sampled at times and locations coincident to the measurements, except that the model vertical layers are kept for clarity. Horizontal lines indicate one standard deviation. Also shown in each panel are the city name, longitude, latitude, number of profiles and mean model biases below 9 km (the mean tropopause height). The black dot in each panel depicts the average tropopause height calculated from the two-way coupled model.

Two-way coupled simulation of tropospheric ozone

Y.-Y. Yan et al.

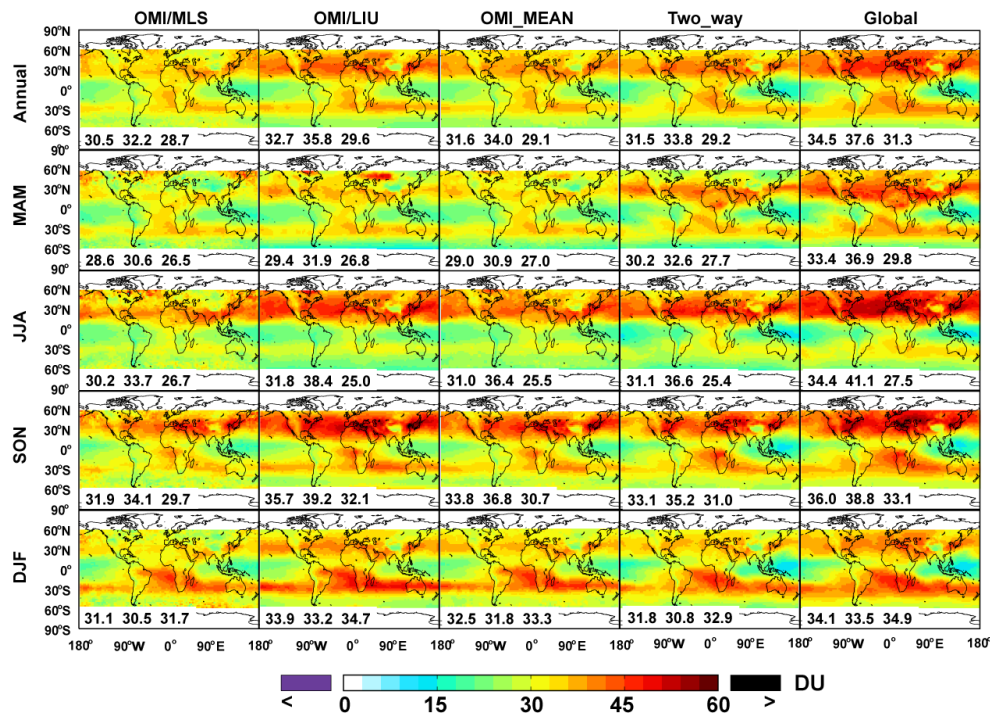


Figure 10. Measured and modeled annual and seasonal mean tropospheric ozone columns from 60° S to 60° N in 2009: (from left to right) OMI/MLS, OMI retrieval by Liu et al. (2010), average of the two satellite datasets, simulation of the two-way coupled system, and simulation of the global model alone. Also shown in each panel are global, NH, and SH means.

Title Page

Abstract Introduction

Conclusions References

Tables Figures

◀ ▶

◀ ▶

Back Close

Full Screen / Esc

Printer-friendly Version

Interactive Discussion



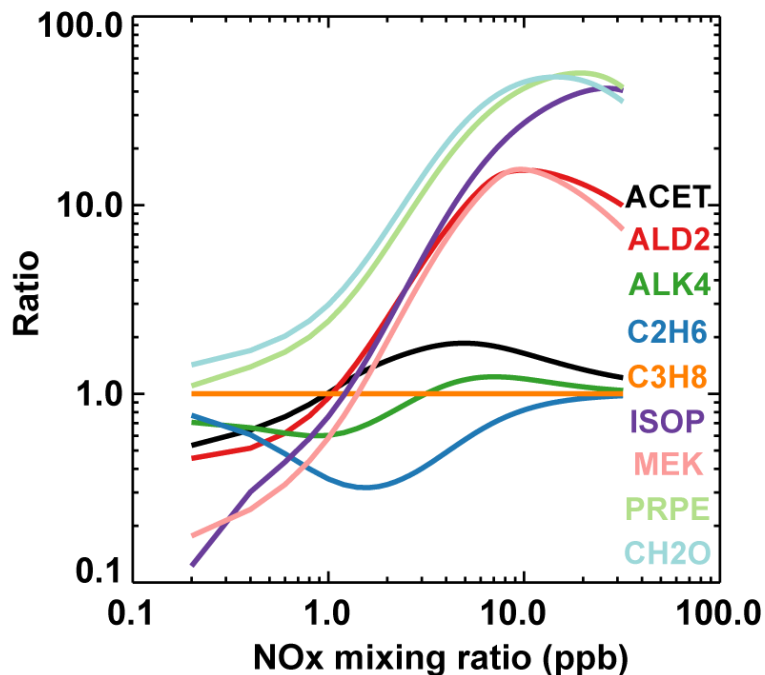


Figure A1. The $P_{O_3}(\text{NMVOC}) / P_{O_3}(\text{C}_3\text{H}_8)$ ratios as a function of initial NO_x levels simulated by DSMACC for nine emitted NMVOCs (C_2H_6 : ethane; C_3H_8 : propane; CH_2O : formaldehyde; ISOP: isoprene; MEK: methyl ethyl ketone; ALK_4 : $\geq \text{C}_4$ alkanes; ACET: acetone; ALD_2 : acetaldehyde; PRPE: propene). The ratios are derived for clear-sky summer noontime (12:00–13:00 LT) with the initial NMVOC level set at 10 ppbC and ozone at 30 ppb. To derive the ratio for a given NMVOC, other NMVOCs are set as zero.

Two-way coupled simulation of tropospheric ozone

Y.-Y. Yan et al.

Title Page

Abstract

Introduction

Conclusions

References

Tables

Figures

◀

▶

◀

▶

Back

Close

Full Screen / Esc

Printer-friendly Version

Interactive Discussion



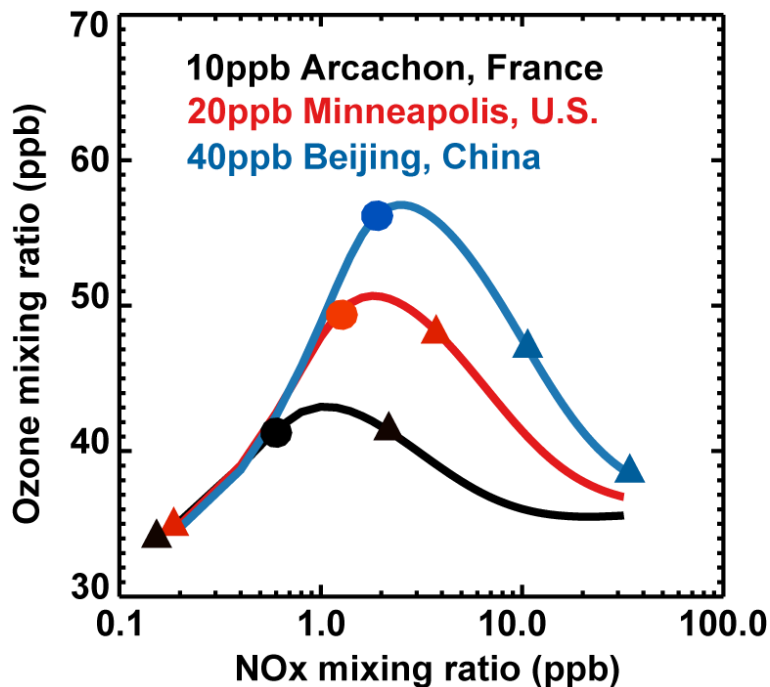


Figure A2. Ozone concentrations as a function of initial NO_x levels after a 1-hour simulation of the DSMACC box model. The simulation is done at clear-sky summer noontime (12:00–13:00 LT) with an initial ozone level at 30 ppb and three initial levels of propane approximately representing the conditions for the three cities in Table A1. Corresponding to Table A1, for each city, the filled circle indicates the NO_x level over the city simulated by the coarse global model, and the two filled triangles represent the NO_x levels over the city and its surroundings, respectively, simulated by the one-way nested models.

Title Page	
Abstract	Introduction
Conclusions	References
Tables	Figures
◀	▶
◀	▶
Back	Close
Full Screen / Esc	
Printer-friendly Version	
Interactive Discussion	

